Journal of Biomedical Optics

SPIEDigitalLibrary.org/jbo

# Photoacoustic tomography of *ex vivo* mouse hearts with myocardial infarction

Markus Holotta
Harald Grossauer
Christian Kremser
Pavle Torbica
Jakob Völkl
Gerald Degenhart
Regina Esterhammer
Robert Nuster
Günther Paltauf
Werner Jaschke

SPIE

# Photoacoustic tomography of *ex vivo* mouse hearts with myocardial infarction

**Markus Holotta,[a] Harald Grossauer,[b] Christian Kremser,[a] Pavle Torbica,[a] Jakob Völkl,[c] Gerald Degenhart,[a] Regina Esterhammer,[a] Robert Nuster,[d,e] Günther Paltauf,[d] and Werner Jaschke[a]**
[a]Innsbruck Medical University, Department of Radiology, Anichstrasse 35, 6020 Innsbruck, Austria
[b]University of Innsbruck, Department of Mathematics, Technikerstraße 15, 6020 Innsbruck, Austria
[c]Innsbruck Medical University, Department of Internal Medicine – Cardiology, Anichstrasse 35, 6020 Innsbruck, Austria
[d]Karl-Franzens-University Graz, Department of Physics, Hafenstraße 47-51, 4020 Linz, Austria
[e]RECENDT GmbH, Department of Sensor Technology, Universitätsplatz 5, 8010 Graz, Austria

**Abstract.** In the present study, we evaluated the applicability of *ex vivo* photoacoustic imaging (PAI) on small animal organs. We used photoacoustic tomography (PAT) to visualize infarcted areas within murine hearts and compared these data to other imaging techniques [magnetic resonance imaging (MRI), micro-computed tomography] and histological slices. In order to induce ischemia, an *in vivo* ligation of the left anterior descending artery was performed on nine wild-type mice. After varying survival periods, the hearts were excised and fixed in formaldehyde. Samples were illuminated with nanosecond laser pulses delivered by a Nd:YAG pumped optical parametric oscillator. Ultrasound detection was achieved using a Mach–Zehnder interferometer (MZI) working as an integrating line detector. The voxel data were computed using a Fourier-domain based reconstruction algorithm, followed by inverse Radon transforms. The results clearly showed the capability of PAI to visualize myocardial infarction and to produce three-dimensional images with a spatial resolution of approximately 120 $\mu$m. Regions of affected muscle tissue in PAI corresponded well with the results of MRI and histology. Photoacoustic tomography utilizing a MZI for ultrasound detection allows for imaging of small tissue samples. Due to its high spatial resolution, good soft tissue contrast and comparatively low cost, PAT offers great potentials for imaging.
© *2011 Society of Photo-Optical Instrumentation Engineers (SPIE)*. [DOI: 10.1117/1.3556720]

Keywords: photoacoustic imaging; mouse; myocardial infarct; laser; noninvasive.

Paper 10627PR received Nov. 26, 2010; revised manuscript received Jan. 21, 2011; accepted for publication Jan. 27, 2011; published online Mar. 9, 2011.

## 1 Introduction

Photoacoustic (sometimes called optoacoustic) imaging (PAI) is becoming a major tool for preclinical studies owing to its unique property of combining aspects of optical and ultrasound imaging. PAI is based on the thermoelastic effect, which means that an acoustic wave is produced inside a sample due to local heating and rapid expansion caused by short pulses of radiation, usually laser pulses in the nanosecond range.[1] Its potential for *in vitro* and *in vivo* imaging has been demonstrated both in photoacoustic tomography (PAT) setups and in photoacoustic microscopy.[2,3] PAI is considered a new imaging technique that can be applied to many fields of biomedical imaging. The noninvasive and nonionizing character of this technique makes it ideal for *in vivo* studies in biological and medical research.

Because the technique is sensitive to small changes in optical absorption, spectrally resolved PAT allows for noninvasive measurement of tissue oxygenation *in vivo*, which can be used to study metabolism and tissue viability noninvasively.[4] Apart from the contrast caused by endogenous chromophores such as hemoglobin, exogenous contrast materials such as nanoparticles can also be visualized by PAT and may provide additional information on tissue characteristics.[5,6] In addition, photoacoustic imaging has the potential to produce images in which contrast is based on molecular differences within tissues.[5] Thus, molecular imaging may be another field of application for PAI.

We investigated if PAT can produce images with appropriate spatial and contrast resolution of small animal organs and if PAT can visualize myocardial infarction in *ex vivo* mouse hearts. The PAT results were compared to magnetic resonance imaging (MRI), micro-computed tomography ($\mu$CT) and histology.

## 2 Materials and Methods

### 2.1 *Sample Preparation*

In order to induce a myocardial infarction, the left anterior descending artery of wild type C57Bl6/N mice was ligated *in vivo* in a similar way described elsewhere, but without reperfusion.[7] Mice were sacrificed and hearts were excised after 3, 5, and 7 days. After excision, hearts were immediately transferred into a 4% formaldehyde solution for conservation. To enable mounting on the translation stage, they were embedded into 12% agar and attached to a small stick (Fig. 1).

After completion of the different imaging procedures, three 5 $\mu$m sections were cut at a distance of 1 mm from the apex to the midsection of the left ventricle for hematoxylin and eosin

Address all correspondence to: Markus Holotta, Innsbruck Medical University, Department of Diagnostic Radiology, Center of Diagnostic Radiology, Anichstrasse 35, 6020 Innsbruck, Austria. Tel: +43 512 507 26219; Fax: +43 512 507 22758; E-mail: markus.holotta@i-med.ac.at.

1083-3668/2011/16(3)/036007/5/$25.00 © 2011 SPIE

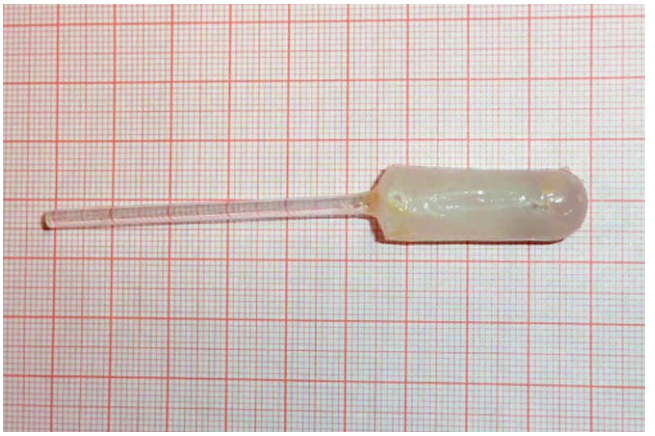

**Fig. 1** Photograph of a murine heart embedded in agar.

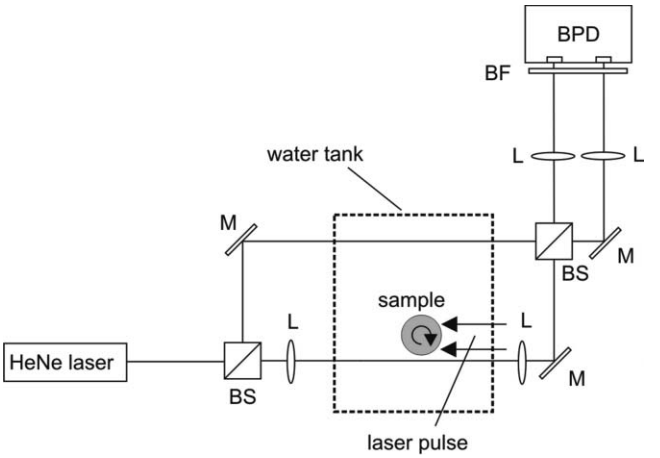


**Fig. 2** Schema of the experimental setup. BS: beam splitter, M: mirror, BPD: balanced photodetector, L: lens, BF: band pass filter. (Modified after Paltauf et al. 2007, with permission.)

staining. The size of the hearts was about 12 mm × 8 mm. Animals were handled in accordance with institutional guidelines and all experiments were approved by the Institutional Ethics Committee and in accordance with the Guide for the Care and Use of Laboratory Animals published by the US National Institutes of Health (NIH Publication No. 85-23, revised 1996).

## 2.2 *Experimental Setup*

In our setup, the measurement of the pressure wave was performed by a Mach–Zehnder interferometer (MZI) acting as an integrating line detector. A beam splitter was used to split the laser beam coming from a HeNe-laser into two beams—the reference beam and the measurement beam. Both beams passed through a water tank and were brought to interference after the tank. To provide acoustic coupling, the sample was submerged into the water tank close to the measurement beam. For photoacoustic (PA) signal generation, laser pulses with a pulse duration of about 5 ns from an optical parametric oscillator (Continuum® Surelite OPO Plus, Continuum, Santa Clara, CA) pumped by a frequency tripled Q-switched Nd:YAG laser (Continuum® Surelite 10 II, Continuum, Santa Clara, CA) were fired at the sample at a repetition rate of 10 Hz. The pressure waves emanating from the sample led to local changes in the refractive index of the water, causing the phase of the measurement beam to shift relative to the reference beam. When bringing the two laser beams to interference, the phase shift caused oscillations in the intensity of the combined beam, which were measured by a balanced photodetector (Thorlabs PDB120A, Thorlabs GmbH, Dachau, Germany) and recorded without averaging on a digital oscilloscope (LeCroy Waverunner 64Xi, LeCroy Corporation, Chestnut Ridge, New York) (Fig. 2). These measurements were repeated numerous times as the sample was moved around the measurement beam. A more detailed description of PAT using a MZI can be found in the work of Paltauf et al.[8] and Nuster et al.[9]

The samples were continuously illuminated by laser pulses guided through a glass fiber (1 mm diameter) from one side, moved around the interferometer beam by two linear translation stages, and turned by a rotation stage. The laser spot size was adjusted by a lens to cover the whole heart and had a diameter of approximately 1 cm. The radiant energy at the sample was about 10 mJ/cm$^2$.

The scan geometry (box-scan) was a combination of three linear scans and looked like a bottomless box with a side length of 17 mm (Fig. 3). Every 60 $\mu$m along one side, a full rotation of the sample was performed at a speed that resulted in 229 detection points around the circle and an angular increment of about 1.57 deg. Single signals were recorded without averaging at each of the 194,650 detection points. The scan time with the given parameters was around 4.5 h.

If the detector positions were located along a straight line, as for example on each side of a box-scan, an exact reconstruction could be achieved by a Fast Fourier Transform method.[10] For this study, we exclusively performed box-scans, since the positioning of the sample in this case was quite easy and the reconstruction was fast and robust. To keep the effects of acoustic attenuation of the pressure wave small, the sample was guided as close as possible to the measurement beam. For mechanical reasons, we could not measure the entire way around the sample, because at some point the mounting of the sample would have blocked the measurement laser beam. Therefore, no measurement data for the lower side of the scan were achievable. The corresponding limited view problem is discussed elsewhere.[11]

The validation of imaging properties of our system was done by measuring blue sutures made of monofilamentous

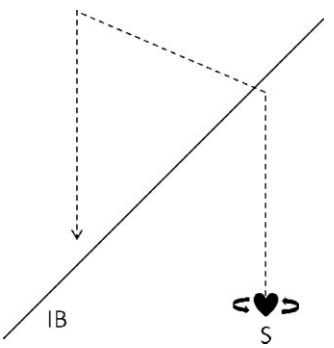


**Fig. 3** Sketch of the scan geometry. IB: interferometer beam, S: sample.

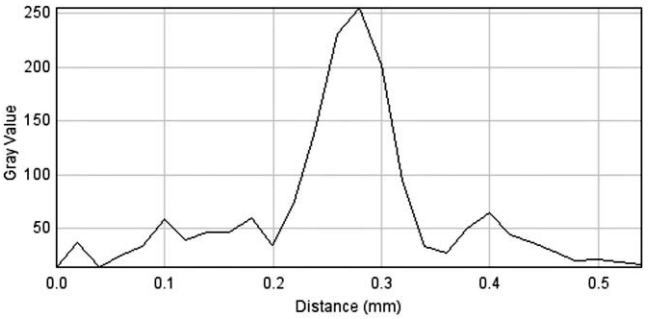


**Fig. 4** Gray scale profile of a sutures cross section.

polypropylene with a diameter of 70 $\mu$m (Prolene®, Ethicon, Inc., Norderstedt, Germany) with different measurement parameters. At each of the two chosen wavelengths (520 and 750 nm), we first applied the same step width (60 $\mu$m) and angular increment ($\sim$1.57 deg, resulting in 229 detection points) as used in the heart measurements. In further trials, we reduced the angular increment to 1 deg. The theoretical resolution limit was given by the waist-diameter of the focused measurement beam.

The determination of spatial resolution was done according to Su et al.[12] The grayscale profile of a suture cross section was used to measure the full width at half maximum of its signal. Because the suture had a diameter of only 70 $\mu$m, it could be regarded as a point absorber allowing for measuring a point spread function.

Magnetic resonance imaging was performed on a standard 1.5T clinical whole body system (Magnetom Avanto, Siemens, Erlangen, Germany) using a linearly polarized small-loop receive coil (inner diameter 28 mm). For imaging of the *ex vivo* mouse heart, a T2 weighted 3D turbo spin echo sequence was used with the following parameters: TR = 2000 ms, TE = 72 ms, turbo factor: 21, echo spacing: 18 ms, receive bandwidth: 102 Hz/pixel, slab thickness: 9.6 mm, number of slices: 16, effective slice thickness: 600 $\mu$m, acquisition field of view (FOV): 40 mm × 40 mm, acquisition matrix 230 × 256, pixel spacing: 195 $\mu$m × 195 $\mu$m, number of averages: 1, total acquisition time: 7 min 02 s.

Computed tomography (CT) scans were performed on a $\mu$CT scanner (vivaCT 40, Scanco Medical AG, Brüttisellen, Switzerland). For the imaging of the mouse hearts, a soft tissue sequence with the following parameters was used: coil voltage = 45 kV; coil electricity = 88 $\mu$A; slice thickness: 60 $\mu$m; FOV: 30.72 mm × 30.72 mm; matrix: 512 × 512; integration time: 220 ms. Acquisition time depended on the sample size and the number of slices and varied from 8–12 min.

## 3 Results

Test measurements with blue sutures at different wavelengths and with different angular increments revealed that neither the wavelength nor the number of chosen detection points (229 or 360) were crucial for the resolution of the setup. The advantage of more detection points was a higher signal to noise ratio and a better perceptibility of low contrast structures, resulting from more effective filtering and averaging during reconstruction, at the cost of scan time. The spatial resolution of the system was determined on the basis of a gray scale profile of a suture cross section. The profile is shown in Fig. 4. A point spread function applied on the gray scale profile revealed a resolution of about 120 $\mu$m. The true resolution given by the point spread function might be slightly overestimated by this value, due to the finite width of the sample.

Scans of nine hearts from mice with varying survival times at wavelengths in the visible and near infrared spectrum (500–1000 nm) were performed to find a wavelength that provided the best tissue contrast. For the detection of ischemic tissue in mouse hearts, a wavelength around 750 nm delivered the best results. Slices shown in each figure are at approximately the same imaging plane.

The ischemic regions in the photoacoustic images [marked by arrows in Figs. 5(b), 6(b), and 7(b)] were characterized by lower absorption compared to the surrounding healthy muscle tissue in the myocardial wall. In T2 weighted magnetic resonance (MR) images, these parts were characterized by brighter shades of gray compared to the unaffected myocardium, which appeared as almost black [marked by arrows in Figs. 5(a), 6(a), and 7(a)]. Agar has high water content and has, depending on its concentration, almost the same optical properties as water. Therefore, it was not visible in the photoacoustic images but was visible in the MR images [Figs. 5(a), 6(a), and 7(a)]. Hemoglobin has higher optical absorption than water or muscle tissue and therefore gives the strongest signal in PAT images, and was visible in the partly blood-filled left ventricle [Fig. 7(b)]. Due to the poor soft tissue contrast, no details inside the myocardium were visible on $\mu$CT images [Figs. 5(c), 6(c), and 7(c)]. The white

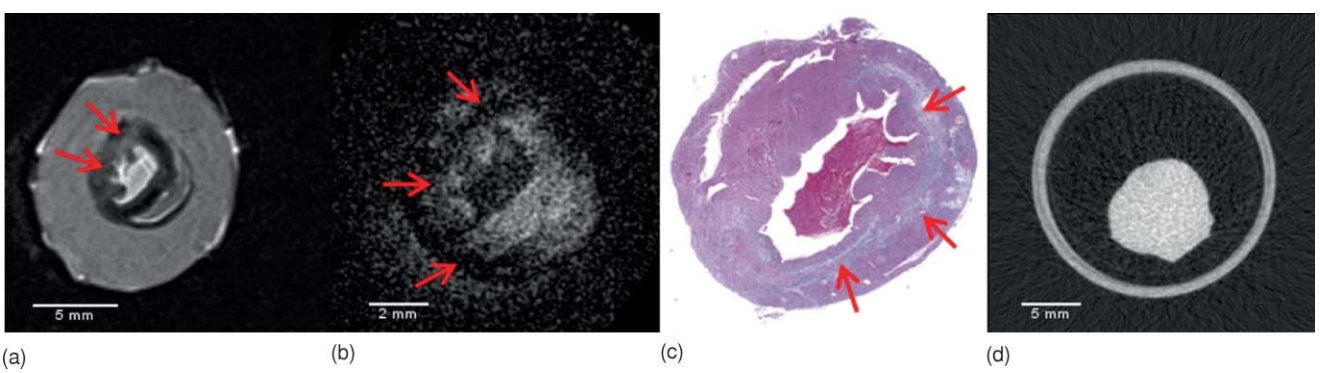


**Fig. 5** Slices of a mouse heart, mouse survived for 3 days. (a) MRI. (b) PAI. (c) Stained histological section. (d) $\mu$CT. Infarcted regions are marked by arrows.

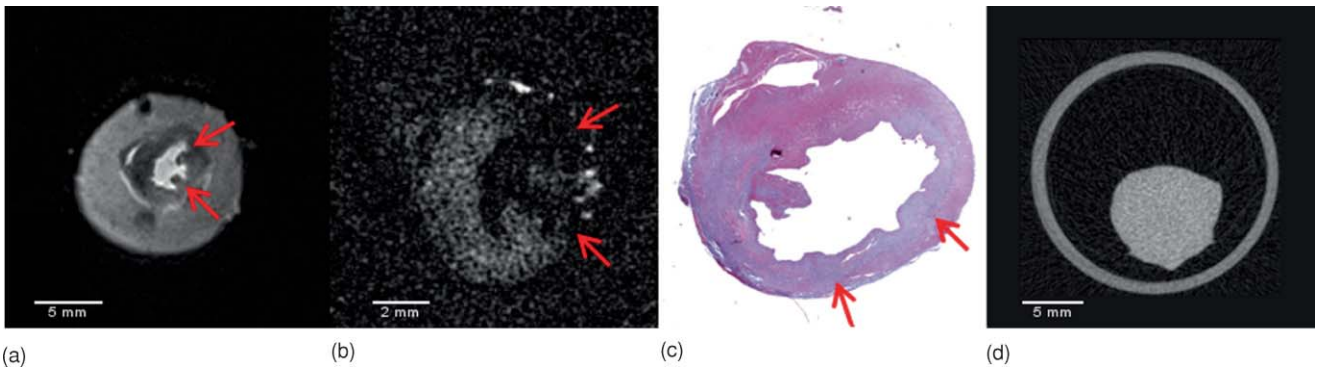


**Fig. 6** Slices of a mouse heart, mouse survived for 5 days. (a) MRI. (b) PAI. (c) Stained histological section. (d) $\mu$CT. Infarcted regions are marked by arrows.

ring around the heart represents the sample holder tube of the $\mu$CT system.

In the haematoxylin and eosin (H&E) stained histological sections, ischemic tissue was represented in shades of blue and marked by arrows [Figs. 5(d), 6(d), and 7(d)]. Although there were some deformations in the histological slices resulting from cutting and staining procedures, infarcted regions corresponded well with the other imaging modalities.

## 4 Discussion

Three-dimensional, high-resolution imaging is of paramount interest in clinical and biological research. To our knowledge, this is the first study to compare already established imaging modalities like MRI and $\mu$CT with the relatively new method of photoacoustic imaging. Our current results clearly demonstrate the potential of PAT with integrating line detectors to visualize myocardial infarction *ex vivo*.

In T2 weighted MR images, infarcted myocardium was demonstrated in brighter shades of gray, indicating the presence of intercellular edema, a common occurrence after myocardial infarction.[13] The weaker signal of affected muscle tissue in PAI was a result of lower optical absorption, indicating higher water content and a possibly lower tissue density caused by necrosis. Kawasuji et al. stated in his work that myoglobin and hemoglobin concentration rapidly decreases after coronary occlusion, which would also lead to lower optical absorption in the affected muscle.[14]

*Ex vivo*, $\mu$CT without the application of contrast agents was not capable of delivering adequate soft tissue contrast to visualize early changes in tissue properties after a myocardial infarction. Ventricles were not visible because they were either filled with isodense blood or fixative. MRI provided comparable image quality to PAI concerning tissue differentiation without the use of contrast agents, but featured the lowest spatial resolution among all imaging modalities compared in this study. For an exact determination of the infarct size histological staining methods are still gold standard. H&E staining is a widespread practice in medicine and biology and allows for an exact visualization of the ischemic tissue. Acidophilic components, dominant in infarcted areas, were visualized in blue mainly due to hypereosinophilia, nuclear pyknosis, and karyolysis.

In digital imaging modalities, it is more difficult to define borders between ischemic and healthy tissue. Therefore, a quantitative comparison of the infarct size between histological sections and PAT/magnetic resonance tomography (MRT) was not feasible, not least because of tissue deformation as a result of the preparation process. Nevertheless, we tried to find corresponding slices in each modality on the basis of typical anatomical landmarks. Size and position of structures in PAT and MRT images corresponded well to each other with given PA imaging parameters.

The application of a Mach–Zehnder interferometer enabled ultrasound detection at a high signal to noise ratio and the acquisition of images at a resolution of about 120 $\mu$m under the tested conditions. On the other hand, it limited measurements

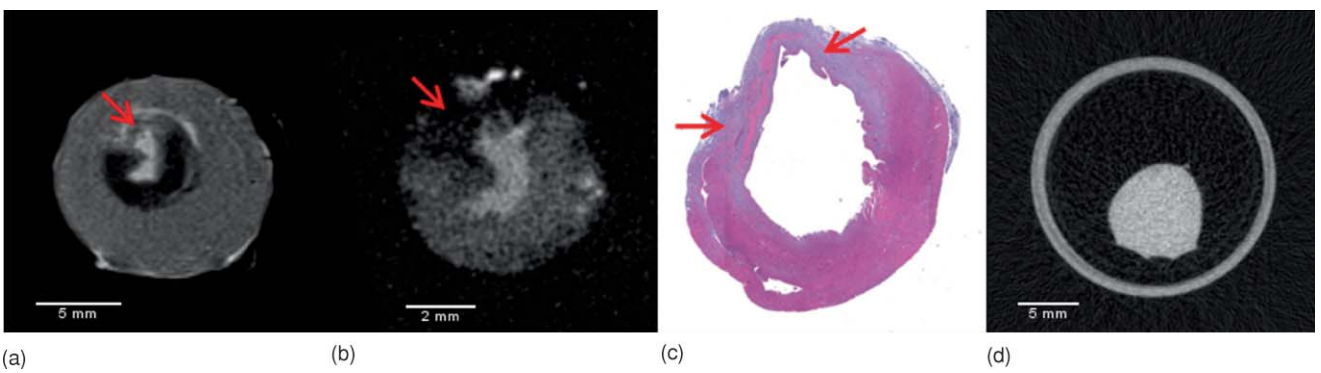


**Fig. 7** Slices of a mouse heart, mouse survived for 7 days. (a) MRI. (b) PAI. (c) Stained histological section. (d) $\mu$CT. Infarcted regions are marked by arrows.

to small *ex vivo* samples, since it required a water tank and the movement of the sample around the interferometer beam. The measurement speed was primarily limited by the repetition rate of the laser but could be accelerated with adequate equipment. For future scans, we will apply a different scanning procedure, where the sample is moved in a 240 deg circular arc around the measurement beam instead of three linear scans. This new procedure, combined with adapted reconstruction algorithms, allows for a reduction in scan time by about two thirds without any loss of image quality. A further reduction of scan time could be achieved by utilization of a laser with a higher repetition rate.

This study was confined to the detection of pathological tissue inside a mouse heart, but using different wavelengths could allow for visualization of other tissue characteristics. Changes in PA signals can be caused by disease, differences in tissue oxygenation, or metabolism. We did not consider the application of contrast-enhancing tracers, because there are no contrast materials that can be used for all imaging modalities applied in this study. It has been shown elsewhere that the usage of contrast-enhancing agents can improve image quality and the field of application of PAI.[5,6]

## Acknowledgments

This study is funded by FWF (Austrian Science Fund), Grant Nos. S10502-N20, S10503-N20, S10504-N20, and S10505-N20.

## References

1. A. C. Tam, "Applications of Photoacoustic Sensing Techniques," *Rev. Mod. Phys.* **58**, 381 (1986).
2. R. A. Kruger, P. Y. Liu, Y. R. Fang, and C. R. Appledorn, "Photoacoustic Ultrasound (Paus)—Reconstruction Tomography," *Med. Phys.* **22**, 1605 (1995).
3. M. Xu and L. V. Wang, "Photoacoustic imaging in biomedicine," *Rev. Sci. Instrum.* **77**, 041101-1 (2006).
4. X. Wang, X. Xie, G. Ku, L. V. Wang, and G. Stoica, "Noninvasive imaging of hemoglobin concentration and oxygenation in the rat brain using high-resolution photoacoustic tomography," *J. Biomed. Opt.* **11**, 024015 (2006).
5. A. De la Zerda, C. Zavaleta, S. Keren, S. Vaithilingam, S. Bodapati, Z. Liu, J. Levi, B. R. Smith, T. J. Ma, O. Oralkan, Z. Cheng, X. Chen, H. Dai, B. T. Khuri-Yakub, and S. S. Gambhir, "Carbon nanotubes as photoacoustic molecular imaging agents in living mice," *Nat. Nanotechnol.* **3**, 557 (2008).
6. Y. Wang, X. Xie, X. Wang, G. Ku, K. L. Gill, D. P. O'Neal, G. Stoica, and L. V. Wang, "Photoacoustic Tomography of a Nanoshell Contrast Agent in the in Vivo Rat Brain," *Nano Lett.* **4**, 1689 (2004).
7. L. H. Michael, M. L. Entman, C. J. Hartley, K. A. Youker, J. Zhu, S. R. Hall, H. K. Hawkins, K. Berens, and C. M. Ballantyne, "Myocardial ischemia and reperfusion: a murine model," *Am. J. Physiol. Heart Circ. Physiol.* **269**, H2147 (1995).
8. G. Paltauf, R. Nuster, M. Haltmeier, and P. Burgholzer, "Photoacoustic tomography using a Mach-Zehnder interferometer as an acoustic line detector," *Appl. Opt.* **46**, 3352 (2007).
9. R. Nuster, M. Holotta, C. Kremser, P. Burgholzer, and G. Paltauf, "Photoacoustic microtomography using optical interferometric detection," *J. Biomed. Opt.* **15**, 021307 (2010).
10. K. P. Koestli, M. Frenz, H. Bebie, and H. P. Weber, "Temporal backward projection of optoacoustic pressure transients using Fourier transform methods," *Phys. Med. Biol.* **46**, 1863 (2001).
11. G. Paltauf, R. Nuster, M. Haltmeier, and P. Burgholzer, "Experimental evaluation of reconstruction algorithms for limited view photoacoustic tomography with line detectors," *Inverse Probl.* **23**, S81 (2007).
12. Y. X. Su, F. Zhang, K. X. Xu, J. Q. Yao, and R. K. K. Wang, "A photoacoustic tomography system for imaging of biological tissues," *J. Phys. D: Appl. Phys.* **38**, 2640 (2005).
13. M. C. Fishbein, D. Maclean, and P. R. Maroko, "The histopathologic evolution of myocardial infarction," *Chest* **73**, 843 (1978).
14. M. Kawasuji, M. Ikeda, N. Sakakibara, S. Fujii, S. Tomita, and Y. Watanabe, "Near-infrared monitoring of myocardial oxygenation during ischemic preconditioning," *Ann. Thorac. Surg.* **69**, 1806 (2000).